IEEE Transactions on Instrumentation and Measurement

Papers are sought that address innovative solutions to the development and use of electrical and electronic instruments and equipment to measure, monitor and/or record physical phenomena for the purpose of advancing measurement science, methods, functionality and applications.

1.808	0.01534	0.546
Impact Factor	Eigenfactor	Article Influence Score

Latest Published Articles

Analysis of the Distortion of Marker-Based Optical Position Measurement as a Function of Exposure Time — Agu-09 2016
Tamás Dabóczi

Correcting Instrumental Variation and Time-Varying Drift: A Transfer Learning Approach With Autoencoders — Agu-09 2016
Ke Yan ; David Zhang

Automated Machine Vision System for Inspecting Cutting Quality of Cubic Zirconia — Agu-09 2016
Wisitporn Ekwongmunkong ; Pradit Mittrapiyanuruk ; Pakorn Kaewtrakulpong

Electrical Resistance Tomography of Conductive Thin Films — Agu-09 2016
Alessandro Cultrera ; Luca Callegaro

A Machine Vision Apparatus and Method for Can-End Inspection — Agu-09 2016
Tiejian Chen ; Yaonan Wang ; Changyan Xiao ; Q. M. Jonathan Wu

Popular Articles

Logarithmic Analog-to-Digital Converters: A Survey — Nov-12 2007
S. Cantarano ; G. V. Pallottino

600-A Test System for Aging Analysis of Automotive Li-Ion Cells With High Resolution and Wide Bandwidth — Jun-07 2016
Patrick Weßkamp ; Peter Haußmann ; Joachim Melbert

Automated Irrigation System Using a Wireless Sensor Network and GPRS Module — Des-05 2013
Joaquín Gutiérrez ; Juan Francisco Villa-Medina ; Alejandra Nieto-Garibay ; Miguel Ángel Porta-Gándara

Characterization of Frequency Stability: A Transfer Function Approach and Its Application to Measurements via Filtering of Phase Noise — Nov-12 2007
Jacques Rutman

Comparison of analog continuum correlators for remote sensing and radio astronomy — Agu-07 2002
O. Koistinen ; J. Lahtinen ; M. T. Hallikainen

Publish in this Journal

Related Journals

Meet Our Editors

IEEE Instrumentation & Measurement Magazine

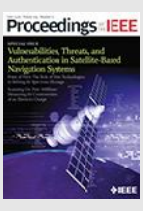

Proceedings of the IEEE

IEEE Access

Editor-in-Chief
Prof. Alessandro Ferrero
Dipartimento di Elettrotecnica
Piazza Leonardo da Vinci 32
Politecnico di Milano
Milano 20133 Italy
alessandro.ferrero@polimi.it
Phone: 39-02-2399-3751
Fax: 39-02-2399-3703

Nurhadi, Hendro

Institut Teknologi Sepuluh Nopember, Department of Ocean Engineering, Surabaya, Indonesia

Author ID: 25646368600

Documents: 12

Citations: 9 total citations by 9 documents

h-index: 1

Co-authors: 14

Subject area: Engineering , Computer Science View More

Analyze author output

View *h*-graph

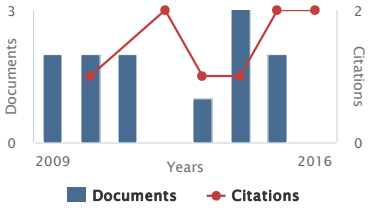

12 Documents | Cited by 9 documents | 14 co-authors

12 documents View in search results format

Sort on: **Date** Cited by ...

Export all | Add all to list | Set document alert | Set document feed

Ensemble kalman filter with a square root scheme (EnKF-SR) for trajectory estimation of AUV SEGOROGENI ITS Show abstract | Related documents	Herlambang, T., Djatmiko, E.B., Nurhadi, H.	2015	International Review of Mechanical Engineering	0
Control simulation of an Automatic Turret Gun based on force control method Show abstract | Related documents	Moh. Nasyir, T., Pramujati, B.,Nurhadi, H. ,Pitowarno, E.	2015	Proceedings of 2014 International Conference on Intelligent Autonomous Agents, Networks and Systems, INAGENTSYS 2014	0
Preliminary numerical study on designing navigation and stability control systems for ITS AUV Show abstract | Related documents	Herlambang, T., Nurhadi, H.,Subchan	2014	Applied Mechanics and Materials	1
Experimental-based TGPID motion control for 2D CNC machine Show abstract | Related documents	Nurhadi, H.,Subowo, Hadi, S.,Mursid, M.	2014	Applied Mechanics and Materials	0
Preliminary study on magnetic levitation modeling using PID control Show abstract | Related documents	Patriawan, D.A., Pramujati, B.,Nurhadi, H.	2014	Applied Mechanics and Materials	0
Sliding-mode (SM) and Fuzzy-Sliding-Mode (FSM) controllers for high-precisely linear piezoelectric ceramic motor (LPCM) Show abstract | Related documents	Nurhadi, H.	2013	Proceedings of 2013 International Conference on Robotics, Biomimetics, Intelligent Computational Systems, ROBIONETICS 2013	0
Multistage rule-based positioning optimization for high-precision LPAT Show abstract | Related documents	Nurhadi, H.	2011	IEEE Transactions on Instrumentation and Measurement	0
Experimental PC based TGPID control method for 2D CNC machine Show abstract | Related documents	Nurhadi, H.,Tarng, Y.-S.	2011	Expert Systems with Applications	1
Study on controller designs for high-precisely linear piezoelectric ceramic motor (LPCM): Comparison of PID-sliding-fuzzy Show abstract | Related documents	Nurhadi, H.,Kuo, W.-M., Tarng, Y.-S.	2010	Proceedings of the 2010 5th IEEE Conference on Industrial Electronics and Applications, ICIEA 2010	0
Two-stage rule-based precision positioning control of a piezoelectrically actuated table Show abstract | Related documents	Kuo, W.M.,Tarng, Y.S., Nian, C.Y.,Nurhadi, H.	2010	International Journal of Systems Science	0
Open- and closed-loop system of computer integrated desktop-scale CNC machine Show abstract | Related documents	Nurhadi, H.,Tarng, Y.-S.	2009	IFAC Proceedings Volumes (IFAC-PapersOnline)	0
Experimental approached optimisation of a linear motion performance with grey hazy set and Taguchi analysis methods (GHST) for ball-screw table type Show abstract | Related documents	Nurhadi, H.,Tarng, Y.-S.	2009	International Journal of Advanced Manufacturing Technology	7

Display 20 results per page

Page 1

Top of page

Author History

Publication range: 2009 - 2015

References: 129

Source history:

Proceedings of 2014 International Conference on Intelligent Autonomous Agents, Networks and Systems, INAGENTSYS 2014 View documents

Applied Mechanics and Materials View documents

Proceedings of 2013 International Conference on Robotics, Biomimetics, Intelligent Computational Systems, ROBIONETICS 2013 View documents

View More

Show Related Affiliations

Multistage Rule-Based Positioning Optimization for High-Precision LPAT

Hendro Nurhadi

***Abstract*—This paper proposes a multistage rule-based precision positioning control method for the linear piezoelectrically actuated table (LPAT). During the coarse-tuning stage, the LPAT is actuated by coarse voltage schemes toward the target of 20 μm at a higher velocity, and during the fine-tuning stage, it is steadily and accurately driven by the fine voltage scheme to reach the target position. The rule-based method is employed to establish the control rules for the voltages and displacements of the two stages using statistical methods. The experimental results demonstrate that the proposed control method can quickly reach steady state, and the steady-state error can be reduced to less than or equal to 0.02 μm for small travel (± 0.1 μm) and large travel (± 20 mm).**

***Index Terms*—Coarse tuning, fine tuning, linear motion, multistage control, optimization, piezoelectrically actuated table, rule-based method (RBM).**

I. Introduction

RECENTLY, the demand for high-accuracy positioning systems has been increasing in the areas of mechanical, electrical, and optical devices. Much attention has been paid to piezoelectric element materials [1]. Traditional piezoelectric actuators have often been utilized to drive a precision positioning table and are classified into three types, namely, frictional actuating device, inchworm device, and material elastic deformation device [2]. The positioning table actuated by frictional actuating and inch-worm devices can achieve a longer stroke, whereas that driven by material elastic deformation device often obtains better positioning precision [3]. A linear piezoelectrically actuated table (LPAT) has been widely used in precision positioning applications, which is driven by the ultrasonic vibration force of piezoelectric ceramic elements and the mechanical friction effect. It has the merits of achieving high precision, being of compact size, being lightweight, achieving high torque and quick responses, and being capable of operating in the presence of electromagnetic fields; above all, it can achieve a movement of longer stroke [4]. However, they also have drawbacks of serious hysteresis behavior and highly nonlinear property, which are difficult to overcome using conventional control strategies [5].

Manuscript received December 9, 2009; revised May 16, 2010; accepted June 10, 2010. Date of publication April 25, 2011; date of current version September 14, 2011. The Associate Editor coordinating the review process for this paper was Dr. Antonios Tsourdos.

The author is with the Department of Mechanical Engineering, Institute of Technology Sepuluh Nopember, Surabaya 60111, Indonesia (e-mail: hdnurhadi@me.its.ac.id).

Color versions of one or more of the figures in this paper are available online at http://ieeexplore.ieee.org.

Digital Object Identifier 10.1109/TIM.2011.2128550

In the early 1970s, Newell and Simon from Carnegie-Mellon University proposed a production system model (the foundation of the modern rule-based expert system). The production model is based on the idea that humans solve problems by applying their knowledge (expressed as production rules) to a given problem represented by problem-specific information. A rule-based expert system has five components: 1) the knowledge base; 2) the database; 3) the inference engine; 4) the explanation facilities; and 5) the user interface [6]. Kang *et al.* [7] employed fuzzy rule bases to improve the nonlinearity of a piezoelectrically actuated table. Zhao and Qing [8] used a rule base to increase the stability of nonlinear control systems. Moudgal *et al.* [9] developed a hierarchical rule-based controller to achieve very good performance of a two-link flexible robot. An application of the multistage algorithm is described by Taur *et al.* [18], Keller *et al.* [19], and Hasiewicz [20].

Many different methods for positioning control applied to the same LPAT as we use have been proposed in previous studies [10]–[14] to resolve the hysteresis behavior and the uncertainty issues. A comparison of these different approaches and the results thus obtained is as follows: Sung and Huang [10] designed a three-stage fuzzy controller. The membership function was divided into three areas (i.e., coarse-tuning area, transitional-tuning area, and fine-tuning area) to improve the effects of nonlinearity and high-frequency chattering of an LPAT. At the beginning of a step response, the error is large, and the controller will choose the largest division of membership (coarse-tuning area). Finally, the controller will switch the range of membership function to the fine-tuning area to correct the steady-state error. Comparing the fuzzy control and the PID control after the third-order polynomial trajectory experiments, the PID control performance was improved from the original steady-state error of 0.5–2.5 to 0.1–0.2 μm and the maximum lag of 13–32 to 6–15 μm. Wai and Lee [11] proposed a double-inductance double-capacitance resonant driving circuit and a four-layer sliding-mode fuzzy-neural-network (FNN) controller, which comprises an FNN controller and a robust controller. The FNN controller is used to learn the equivalent control law in conventional sliding mode due to the unknown system dynamics, and the robust controller is designed to curb the controlled system dynamics on the sliding surface for all time (as $t \to \infty$). The mixed reference trajectories, which are a periodic step command with 1-cm stroke before 10 s and a periodic sinusoidal command with 2-cm stroke after 10 s, are adopted to test the control characteristics of the proposed control scheme. The maximum tracking error of the examined cases is 1.06 mm. The percentage tracking error is less than 3%. Wai and Su [12] also developed a supervisory genetic

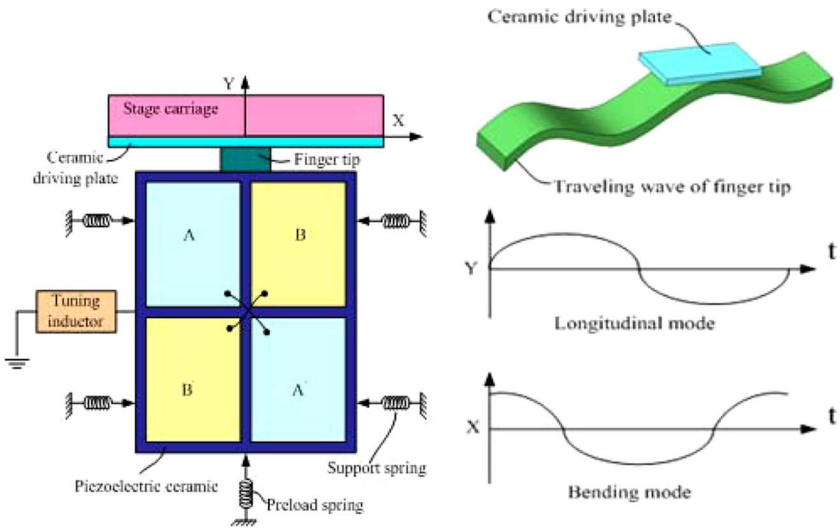

Fig. 1. Structure and actuating mode of the piezoelectric actuator.

algorithm (GA) to improve the nonlinearity of an LPAT, which is composed of two parts: 1) a GA control for searching an optimal control effort online via a gradient descent training process, and 2) a supervisory control for stabilizing the system states around a predefined bound region. With this, the mixed reference trajectory obtained is a periodic sinusoidal command with $\pm$1- and 2-cm strokes, and the maximum tracking error is 0.66 mm. In another study, Wai [13] used an adaptive grey control system to achieve a grey uncertainty predictor and estimate the lumped uncertainty online to relax the requirement of the unknown uncertainty in the design of a computed torque position controller. He obtained a periodic sinusoidal command with 2-cm amplitude, and the tracking error is about 1.5 mm. Lin and Peng [14] proposed an adaptive cerebellar model articulation controller (CMAC)-based supervisory control system to attenuate the tracking error caused by modeling uncertainties. In this design, if the adaptive CMAC can maintain the system states within the constraint set, then the supervisory controller will be idle. Otherwise, the supervisory controller starts working to force the states back to the constraint set. Their experiment obtained a periodic step reference trajectory with amplitude of 3.5 cm and a maximum error of about 0.84 mm (2.4%). It has been shown that the design of an accurate positioning controller is still difficult owing to the nonlinearity and hysteresis of the piezoelectric motor, as well as the relatively static friction acting on the LPAT by the preload and the vertical weight. In view of this, this paper proposes a new and simple multistage precision positioning control method for the LPAT. During the coarse-tuning stage (CTS), the LPAT is actuated by coarse voltage schemes toward the target of 20 μm at a higher velocity, and during the fine-tuning stage (FTS), it is steadily and accurately driven by fine voltage schemes to reach the target position. The rule-based method (RBM) is employed to establish the control rules for the voltages and displacements of the two stages using statistical methods without involving complex mathematic modules. The proposed control method can quickly reach steady state, and the steady-state error can be reduced to less than 0.02 μm for both small travel (0.1 μm) and large travel (20 mm).

The proposed method, so called a multistage rule-based precision positioning control that is combined with the analytical statistical method of σ distribution, has shown that the error is minimized using a simple approach. In other words, because of its simplicity (requires no high-skilled effort and complex structure design), it might have a significant improvement on the system's performance. This approach is robust. The robustness is clearly indicated by determining less error values for all strokes, e.g., $\pm$0.1 μm, $\pm$0.1 mm, and $\pm$20 mm. Therefore, the main contributions of this paper will be highly valuable, as detailed and listed in Table IV; it is contributing a reduction of the steady-state errors of -0.02 to $+0.02$ μm. They are the simplicity and its robustness, which in the end will reduce the cost and improve the performance in precisely nanoscale area.

The rest of this paper is organized as follows: Section II describes the driving principle of the LPAT. The experimental setup is presented in Section III. The characteristic experiments on voltage versus velocity are detailed in Section IV. Section V describes the rule-based positioning control method. The experimental results and discussion are presented in Section VI. Finally, Section VII contains the conclusion.

II. Driving Principle

The HR4 piezoelectric motor made by Nanomotion Limited consists of four pieces of thin rectangular piezoelectric ceramic devices divided in two sets. Four electrodes (A, A$'$, B, and B$'$) are bounded to the front face of the device, as shown in the left part of Fig. 1. Each electrode covers one-quarter of the upper surface, and A-A$'$ and B-B$'$ are each connected diagonally by a wire. To increase the travel of the LPAT, the slide track is driven by a fingertip (as shown in Fig. 1) in back-and-forth motion instead of by the piezoelectric element directly. The entire piezoelectric ceramic device is constrained by four support springs and kept in close contact with the moving table by a preload spring. Hence, the friction force between the fingertip and the moving table can be utilized to drive the linear motion of the table.

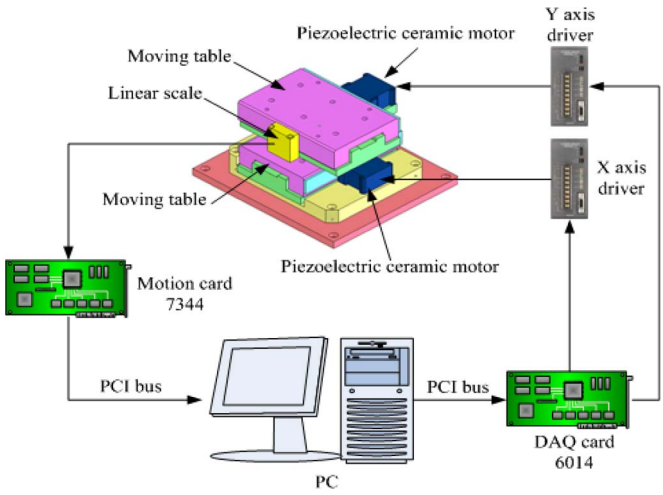

Fig. 2. Experimental setup of the positioning control system.

A command voltage of ± 10 V can be sent to the driver unit and converted to a high sine-wave voltage of 39.6 kHz that drives the motor. The longitudinal and bending modes are generated by the driver, as shown in the right part of Fig. 1. Proper lengths of the piezoelectric ceramic device are selected so that the natural frequency of the two modes are identical, and a circular or oval motion can be produced through the combination of the longitudinal and bending deformations of the device, in addition to the back-and-forth motion induced by the fingertip.

III. Experimental Setup

The experimental setup of this paper includes a table consisting of two HR4 piezoelectric ceramic motors from Nanomotion Limited, two LIE5 linear scales of 20-nm resolution, the independent X-axis table of 150-mm travel, the Y-axis table of 100-mm travel located above the X-axis table, two AB2 drivers, and a 6014 data acquisition (DAQ) card and a 7344 motion card, both of which are made by National Instruments. This paper uses LabVIEW language for the program design.

The control configuration of the entire experiment is plotted in Fig. 2. Initially, the "current position" of the LPAT is detected by linear scale and transmitted to a PC via the motion card, where it is compared with the "target position." The difference between the two positions is then calculated. Proper control voltage corresponding to the position error can be sent to the driver via the DAQ card according to the established control rules of RBM, and then converted into a high sine-wave voltage of 39.6 kHz so as to drive the LPAT. The aforementioned positioning process continues until the position error becomes ± 0.02 μm.

IV. Characteristic Experiments on Voltage Versus Velocity

To investigate the characteristics of the driving voltage, we carried out the characteristic experiments on voltage versus velocity. Fig. 3 shows a block diagram of the characteristic experiments. Two types of voltage, namely, coarse voltage and fine voltage schemes, are used for driving the LPAT. The coarse voltage scheme is a dc voltage and used in CTS, which can be adjusted positively between 1.2 and 1.9 V or negatively between -1.2 and -1.9 V, at intervals of 0.05 V. In this paper, we record the position data once every 10 ms when the LPAT is driven by coarse voltage scheme, as shown in Fig. 3(a). Fig. 3(b) presents the output fine voltage scheme used in FTS, where each output consists of $\tau_{\rm on}$ (voltage is not zero) and $\tau_{\rm off}$ (voltage is zero), and is adjustable between -0.3 and -1.1 V at intervals of 0.05 V. The operating time of each fine voltage scheme step is 30 ms, which includes 10 ms of $\tau_{\rm on}$ and 20 ms of $\tau_{\rm off}$. The operating time is the time needed by a plant to operate; it is different from sampling time.

A. Difference External Voltage Versus Velocity

Difference dc voltages are continuously sent to the X- and Y-axis drivers, respectively, by the DAQ card to drive the corresponding LPAT. Difference input voltages are voltages used for identifying properties of the piezo-materials within the range of working voltage of ± 1.9 V as specified by the manufacturer. The operating time of each output voltage is maintained at 10 ms. Fig. 4(a) displays the velocity response of the X-axis to different voltages, starting from 0 V, increasing to 1.9 V at 0.05-V intervals, then decreasing from 1.9 to -1.9 V also at 0.05-V intervals, and finally increasing to 0 V again at 0.05-V intervals. Fig. 4(b) shows the velocity response of the Y-axis to difference voltages. The experimental processes are the same for the X-axis previously mentioned. As seen in these figures, a flat zone of zero velocity, called the "dead zone," exists in both X- and Y-axes, which is caused by static friction and preload. The dead zone voltage of the X-axis ranges from -1.2 to 1.25 V, whereas that of the Y-axis ranges from -1.15 to 1.15 V.

The LPAT of the X-axis remains stationary until the actuating voltage exceeds 1.25 V in the positive direction or -1.2 V in the negative direction. Hence, 1.25 and -1.2 V are respectively called the "starting voltage" of the X-axis. Similarly, 1.15 and -1.15 V are respectively called the "starting voltage" of the Y-axis. Fig. 4(a) and (b) shows that the LPAT of the X- and Y-axes, respectively, can move very fast and nonlinearly when the driving voltage exceeds the corresponding starting voltage; and the higher the voltage, the greater the velocity will be.

B. Identical Coarse Voltage Scheme Output

"Identical" in this section mentions the signal responses of coarse voltages that have identical responses. To investigate the characteristics of the coarse voltage scheme in detail, 1.3, 1.4, and 1.5 V are selected, respectively, to continuously actuate the LPAT of the X-axis for 2 s, with the velocity responses to different voltages recorded at 10-ms intervals, as shown in Fig. 5. As can be seen, there exists great variation in the 200 velocity responses to each coarse voltage scheme. They seem to be irregular and random, and it is difficult to determine the precise velocity and position at any chosen time when voltages of 1.3, 1.4, and 1.5 V are used to actuate the LPAT.

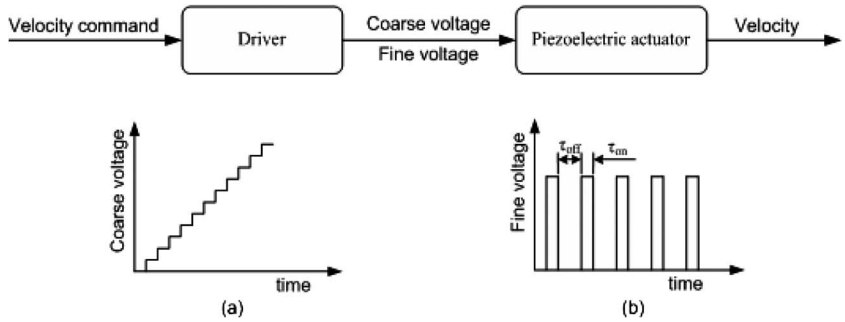

Fig. 3. Block diagram of the characteristic experiment on voltage versus velocity. (a) Coarse voltage schema diagram. (b) Fine voltage schema diagram.

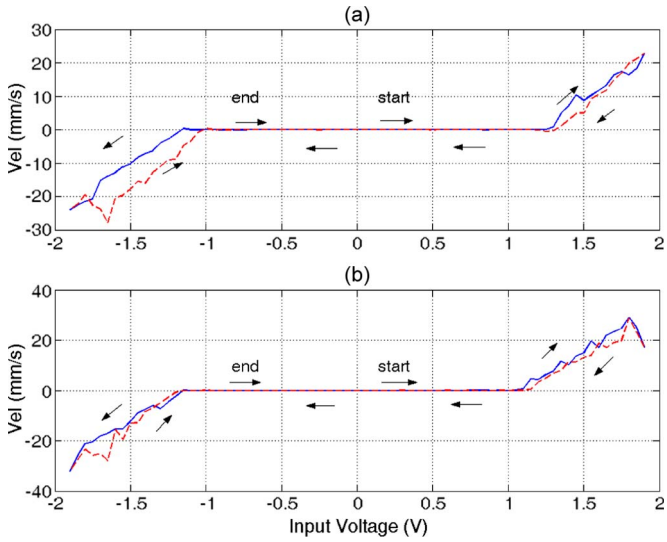

Fig. 4. Velocity responses of the X- and Y-axes to different input voltages. (a) X-axis velocity versus voltage. (b) Y-axis velocity versus voltage.

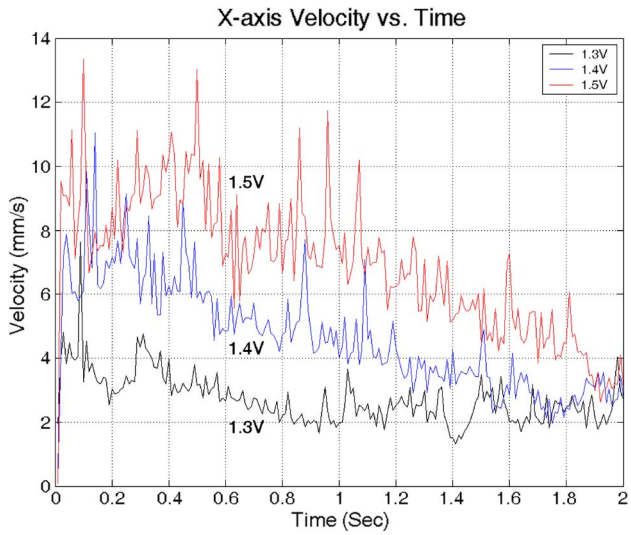

Fig. 5. Velocity responses of the X-axis to identical coarse voltages.

The best that we can do is to find the probable driving range for each voltage [13]. When the LPAT moves closer to the target position, the driving voltage and the relative driving range are both reduced gradually. If the driving range can be less than 0.1 μm, then it may enable the LPAT to reach the target position

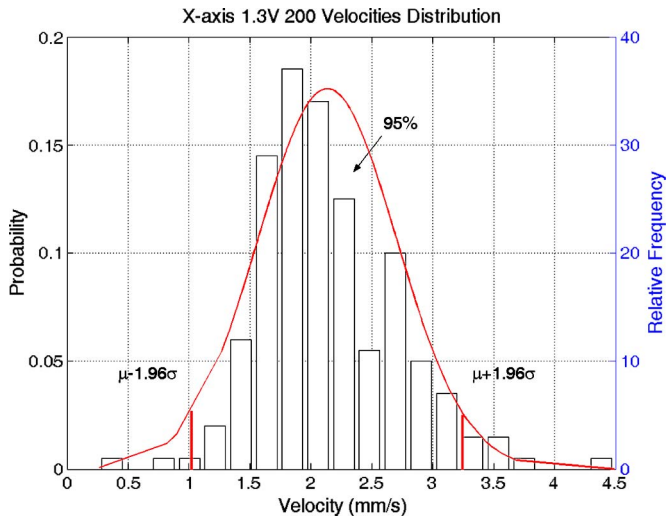

Fig. 6. Statistics of 200 velocity responses to coarse voltage of 1.3 V.

precisely. In this paper, a statistical method is adopted to obtain the probable driving range of each voltage employed.

The most widely used model for the distribution of a random variable is undoubtedly the normal distribution or the Gaussian distribution. Two numbers are often employed to summarize a normal distribution for a random variable x: the mean μ defined in (1) can locate the center of a normal distribution, and the standard deviation σ, which is expressed in (2), can determine the distributive width. Substituting μ and σ into (3) yields the normal probability distribution functions, which represent the probability of an occurrence at x. Equation (4) denotes the cumulative probability in the interval between x_1 and x_2, i.e.,

$$\mu = \frac{1}{n}\sum_{i=1}^{n} Xi \tag{1}$$

$$\sigma = \sqrt{\frac{1}{n-1}\sum_{i=1}^{n}(Xi-\mu)^2} \tag{2}$$

$$f(x) = \frac{1}{\sqrt{2\pi}\sigma} e^{\frac{-(x-\mu)^2}{2\sigma^2}} \tag{3}$$

$$p(x) = \int_{x_1}^{x_2} f(x)dx. \tag{4}$$

From standard normal distribution tables, we can find that the cumulative probability values between $\mu - 1.96\sigma$ (as a

TABLE I
DISPLACEMENT STATISTICS OF TWO AXES FOR TEN COARSE VOLTAGES
[UNIT: μm PER DRIVING TIME (OPERATING TIME = 10 ms)]

X-axis										
Voltage	-1.7V	-1.6V	-1.5V	-1.4V	-1.3V	1.3V	1.4V	1.5V	1.6V	1.7V
Mean(μ)	-0.236	-0.157	-0.092	-0.062	-0.032	0.021	0.047	0.07	0.1	0.148
SD(σ)	0.064	0.042	0.024	0.016	0.009	0.006	0.013	0.022	0.03	0.039
μ+1.96σ	-0.11	-0.074	-0.044	-0.031	-0.016	0.032	0.073	0.112	0.159	0.224
μ-1.96σ	-0.361	-0.24	-0.139	-0.092	-0.048	0.01	0.021	0.027	0.04	0.072
Y-axis										
Voltage	-1.6V	-1.5V	-1.4V	-1.3V	-1.2V	1.2V	1.3V	1.4V	1.5V	1.6V
Mean(μ)	-0.163	-0.132	-0.087	-0.053	-0.016	0.022	0.062	0.086	0.122	0.146
SD(σ)	0.065	0.058	0.032	0.023	0.005	0.007	0.018	0.03	0.048	0.05
μ+1.96σ	-0.036	-0.018	-0.024	-0.009	-0.005	0.035	0.098	0.145	0.216	0.245
μ-1.96σ	-0.291	-0.247	-0.151	-0.098	-0.026	0.009	0.026	0.027	0.028	0.048

TABLE II
DISPLACEMENT STATISTICS OF TWO AXES FOR TEN FINE VOLTAGES
[UNIT: μm PER DRIVING TIME (OPERATING TIME = 30 ms)]

X-axis										
Voltage	-1.1V	-1.0V	-0.7V	-0.4V	-0.3V	0.3V	0.4V	0.7V	1.0V	1.1V
Mean(μ)	-2.44	-1.424	-0.208	-0.157	-0.065	0.041	0.134	0.249	1.348	2.012
SD(σ)	0.846	0.454	0.094	0.05	0.025	0.02	0.051	0.09	0.515	0.785
μ+1.96σ	-0.781	-0.534	-0.024	-0.058	-0.016	0.081	0.235	0.425	2.358	3.551
μ-1.96σ	-4.098	-2.314	-0.392	-0.256	-0.114	0.001	0.034	0.074	0.393	0.473
Y-axis										
Voltage	-1.1V	-1.0V	-0.8V	-0.5V	-0.35V	0.35V	0.5V	0.8V	1.0V	1.1V
Mean(μ)	-2.191	-1.4	-0.226	-0.13	-0.055	0.042	0.113	0.473	1.567	2.352
SD(σ)	0.821	0.47	0.105	0.062	0.022	0.016	0.045	0.125	0.419	0.956
μ+1.96σ	-0.581	-0.479	-0.02	-0.008	-0.012	0.074	0.201	0.718	2.388	4.226
μ-1.96σ	-3.8	-2.321	-0.433	-0.251	-0.098	0.01	0.025	0.228	0.746	0.478

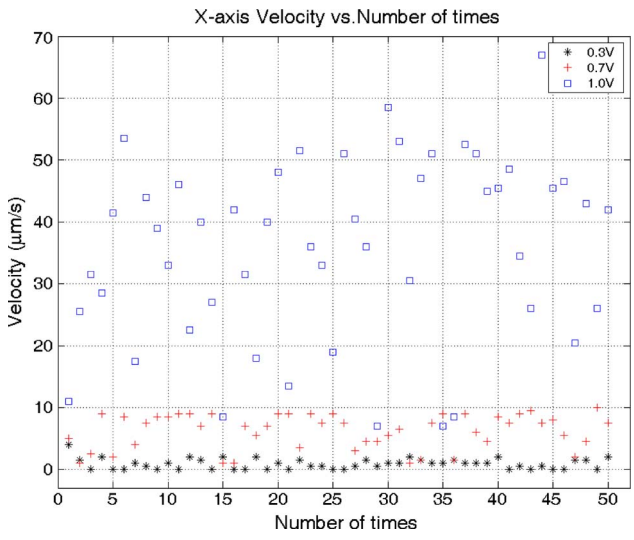

Fig. 7. Velocity responses to fine voltages of 0.3, 0.7, and 1.0 V.

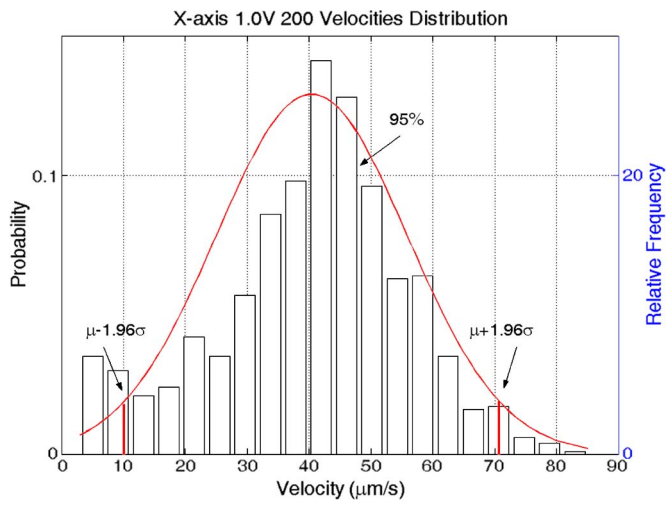

Fig. 8. Velocity statistics (200) of 1.0-V fine voltage.

minimum mean) and $\mu + 1.96\sigma$ (as a maximum mean) are approximately 95%. The most popular uncertainty estimate is that for the 95% confidence; and hence, the ranges of a sample between $\mu - 1.96\sigma$ and $\mu + 1.96\sigma$ are usually regarded as the probable ranges of occurrence [14]. In this paper, the 200 velocity records of 1.3 V seen in Fig. 6 can be converted into a relative frequency distribution histogram and normal distribution, as shown in Fig. 6. As can be seen, the velocity ranges of 1.3 V fall between 1.02 mm/s $(\mu - 1.96\sigma)$ and 3.24 mm/s $(\mu + 1.96\sigma)$ at a 95% confidence level.

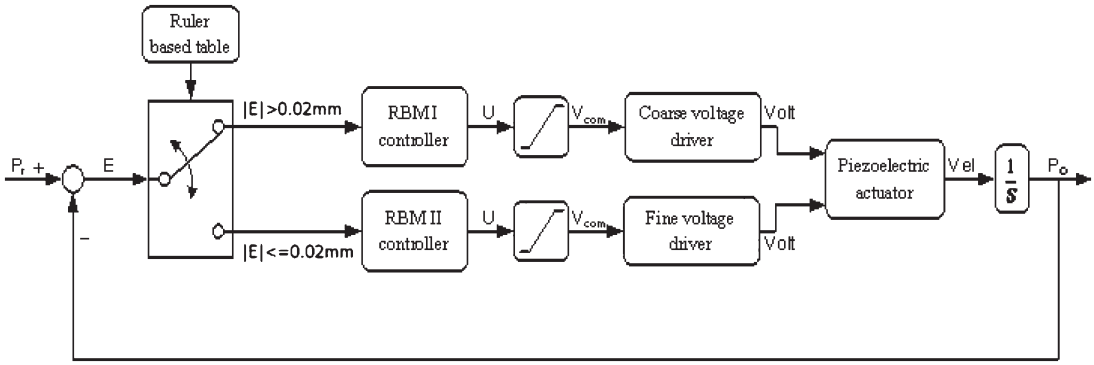

Fig. 9. Block diagram of the positioning experiments.

The aforementioned statistical method is also employed to define the probable corresponding driving displacements of the X- and Y-axes in a driving time (10 ms) for ten different coarse voltage schemes, as listed in Table I.

C. Identical Fine Voltage Scheme Output

As mentioned in Section IV-A, when the coarse driving voltage scheme is higher than the starting voltage of the X- or Y-axis, the LPAT can move quickly. However, when the actuating voltage is lower than the starting voltage, the table remains stationary owing to the static friction and the preload. Nevertheless, when using a fine voltage scheme to actuate the LPAT, such as 0.3–1.1 V shown in Table II, although it is smaller than the starting voltage, the LPAT can still be moved by switching the voltage on and off. Fig. 7 shows the 50 velocity responses of the X-axis to fine driving voltage schemes of 0.3, 0.7, and 1.0 V, respectively, where the driving time of each voltage is 30 ms/step.

Since there still exist a major variation and an uncertainty problem in the 50 velocity records of the identical voltage, the same statistical method described in Section IV-B is thus employed to define the corresponding velocity ranges of an actuated LPAT upon each fine driving voltage scheme to be located between $\mu - 1.96\sigma$ and $\mu + 1.96\sigma$, as shown in Fig. 8. The same statistical method yields the corresponding driving displacements of the X- and Y-axes in an operating time (30 ms) for ten different fine voltage schemes, as listed in Table II.

V. Rule-Based Positioning Control Method

This paper develops a multistage RBM controller. The control block diagram is shown in Fig. 9, and E denotes the position error (E = target position Pr − current position P). When $|\mathrm{E}| > 0.02$ mm, the RBM I controller executes CTS and outputs the corresponding coarse voltage schemes according to the RBM control rules in CTS to drive the LPAT toward the target quickly. If $|\mathrm{E}| \leq 0.02$ mm, the RBM II controller initiates FTS and outputs the corresponding fine voltage schemes according to the RBM control rules in FTS to drive the LPAT stably and accurately toward the target. The characteristic of the coarse voltage scheme is that when it exceeds the relative starting voltage, the motion of the LPAT becomes very sensitive and fast. As seen in Table I, the minimum displacement $(\mu - 1.96\sigma)$ at 1.3 V, the smallest coarse voltage scheme, driving at the X-axis within the driving time (10 ms) is 10.2 μm. While it is too long for precision positioning control, it is excellent for moving the LPAT faster over a long distance within a shorter time. The movement of the LPAT when driven by the fine voltage scheme is slower than when driven by continuous voltage. In Table II, the driven displacement at a fine voltage scheme of 0.3 V ranges from 0.001 μm $(\mu - 1.96\sigma)$ to 0.081 μm $(\mu + 1.96\sigma)$, whereas that at a fine voltage scheme of −0.3 V ranges from −0.016 μm $(\mu - 1.96\sigma)$ to −0.114 μm $(\mu + 1.96\sigma)$ within a driving time of 30 ms. Moving such a short distance each step allows accurate positioning of up to 0.02 μm.

Fig. 10 depicts all the positioning control rules of the X-axis. The numbers under the X-axis denote the value of position errors E. $\mathrm{E} = 0$ indicates that the current position is the target position. As seen in Fig. 10(a), in CTS, the X-axis comprises areas of $|\mathrm{E}| > 0.02$ mm. In the initial positioning control, the position error is large, and a higher continuous voltage is needed for fast movement of the LPAT. When the LPAT approaches the target step by step, the driving continuous voltage should be reduced gradually to avoid bigger overshoot. The main control rule of RBM in CTS is listed as follows:

If $\mathrm{E_x}1_\mathrm{i} \leq \mathrm{E} < \mathrm{E_x}1_{\mathrm{i}+1}$, then the coarse driving voltage scheme is $\mathrm{V_x}1_\mathrm{i}$. ($\mathrm{i} = 1{-}5$ and $\mathrm{i} = 7{-}11$).

The aforementioned values of $\mathrm{E_x}1_\mathrm{i}$ and $\mathrm{V_x}1_\mathrm{i}$ are listed in Table III. The interval of E between −20 and 20 μm is adopted in FTS, as depicted in Fig. 10(b) in detail. The principle of driving is that the smaller the error (E), the smaller the fine driving voltage scheme will be. The main control rule of RBM in FTS is listed as follows:

If $\mathrm{E_x}2_\mathrm{i} \leq \mathrm{E} < \mathrm{E_x}2_{\mathrm{i}+1}$, then the fine driving voltage scheme is $\mathrm{V_x}2_\mathrm{i}$. ($\mathrm{i} = 1{-}11$)

$\mathrm{E_x}2_\mathrm{i}$ and $\mathrm{V_x}2_\mathrm{i}$ are listed in Table III. The method of establishing the rule base for the Y-axis is similar to that for the X-axis. All the positioning control rules of CTS and FTS are detailed in Fig. 11. The main control rules of RBM in CTS and FTS are listed as follows:

If $\mathrm{E_y}1_\mathrm{i} \leq \mathrm{E} < \mathrm{E_y}1_{\mathrm{i}+1}$, then the coarse driving voltage scheme is $\mathrm{V_y}1_\mathrm{i}$. ($\mathrm{i} = 1 \sim 11$)

If $\mathrm{E_y}2_\mathrm{i} \leq \mathrm{E} < \mathrm{E_y}2_{\mathrm{i}+1}$, then the fine driving voltage scheme is $\mathrm{V_y}2_\mathrm{i}$. ($\mathrm{i} = 1 \sim 11$)

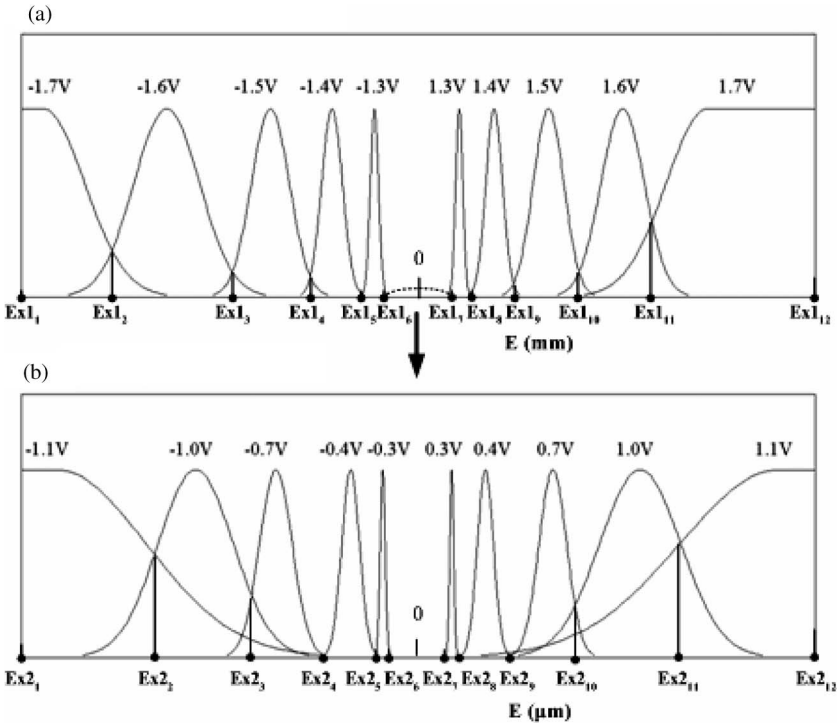

Fig. 10. Control areas of two stages on the X-axis. (a) Area of coarse tuning. (b) Area of fine tuning.

TABLE III
RULE-BASED TABLE FOR X- AND Y-AXES

X-axis											
$Ex1_1$	$Ex1_2$	$Ex1_3$	$Ex1_4$	$Ex1_5$	$Ex1_6$	$Ex1_7$	$Ex1_8$	$Ex1_9$	$Ex1_{10}$	$Ex1_{11}$	$Ex1_{12}$
-∞	-1.82 mm	-0.86 mm	-0.30 mm	-0.12 mm	-0.02 mm	0.02 mm	0.084 mm	0.23 mm	0.678 mm	1.314 mm	∞
$Vx1_1$	$Vx1_2$	$Vx1_3$	$Vx1_4$	$Vx1_5$	Enter	$Vx1_7$	$Vx1_8$	$Vx1_9$	$Vx1_{10}$	$Vx1_{11}$	
-1.7V	-1.6V	-1.5V	-1.4V	-1.3V	FTS	1.3V	1.4V	1.5V	1.6V	1.7V	
$Ex2_1$	$Ex2_2$	$Ex2_3$	$Ex2_4$	$Ex2_5$	$Ex2_6$	$Ex2_7$	$Ex2_8$	$Ex2_9$	$Ex2_{10}$	$Ex2_{11}$	$Ex2_{12}$
-20 μm	-5.88 μm	-1.24 μm	-0.44 μm	-0.16 μm	-0.02 μm	0.02 μm	0.1 μm	0.34 μm	1.22 μm	5.96 μm	20 μm
$Vx2_1$	$Vx2_2$	$Vx2_3$	$Vx2_4$	$Vx2_5$	$Vx2_6$	$Vx2_7$	$Vx2_8$	$Vx2_9$	$Vx2_{10}$	$Vx2_{11}$	
-1.1V	-1.0V	-0.7V	-0.4V	-0.3V	0V	0.3V	0.4V	0.7V	1.0V	1.1V	
Y-axis											
$Ey1_1$	$Ey1_2$	$Ey1_3$	$Ey1_4$	$Ey1_5$	$Ey1_6$	$Ey1_7$	$Ey1_8$	$Ey1_9$	$Ey1_{10}$	$Ey1_{11}$	$Ey1_{12}$
-∞	-1.86 mm	-0.87 mm	-0.27 mm	-0.07 mm	-0.02 mm	0.02 mm	0.09 mm	0.29 mm	0.87 mm	1.73 mm	∞
$Vy1_1$	$Vy1_2$	$Vy1_3$	$Vy1_4$	$Vy1_5$	Enter	$Vy1_7$	$Vy1_8$	$Vy1_9$	$Vy1_{10}$	$Vy1_{11}$	
-1.6V	-1.5V	-1.4V	-1.3V	-1.2V	FTS	1.2V	1.3V	1.4V	1.5V	1.6V	
$Ey2_1$	$Ey2_2$	$Ey2_3$	$Ey2_4$	$Ey2_5$	$Ey2_6$	$Ey2_7$	$Ey2_8$	$Ey2_9$	$Ey2_{10}$	$Ey2_{11}$	$Ey2_{12}$
-20 μm	-5.94 μm	-1.28 μm	-0.4 μm	-0.12 μm	-0.02 μm	0.02 μm	0.1 μm	0.32 μm	1.76 μm	6.56 μm	20 μm
$Vy2_1$	$Vy2_2$	$Vy2_3$	$Vy2_4$	$Vy2_5$	$Vy2_6$	$Vy2_7$	$Vy2_8$	$Vy2_9$	$Vy2_{10}$	$Vy2_{11}$	
-1.1V	-1.0V	-0.8V	-0.5V	-0.35V	0V	0.35V	0.5V	0.8V	1.0V	1.1V	

E_y1_i, E_y2_i, V_y1_i, and V_y2_i are listed in Table III. In addition, another reason why the steady-state error of the proposed controller can easily reach 0.02 μm is attributed to the driving process in FTS. The proper fine voltage schemes selected according to RBM are sent to actuate the LPAT and are maintained constant at 10 ms. The output voltage is then converted

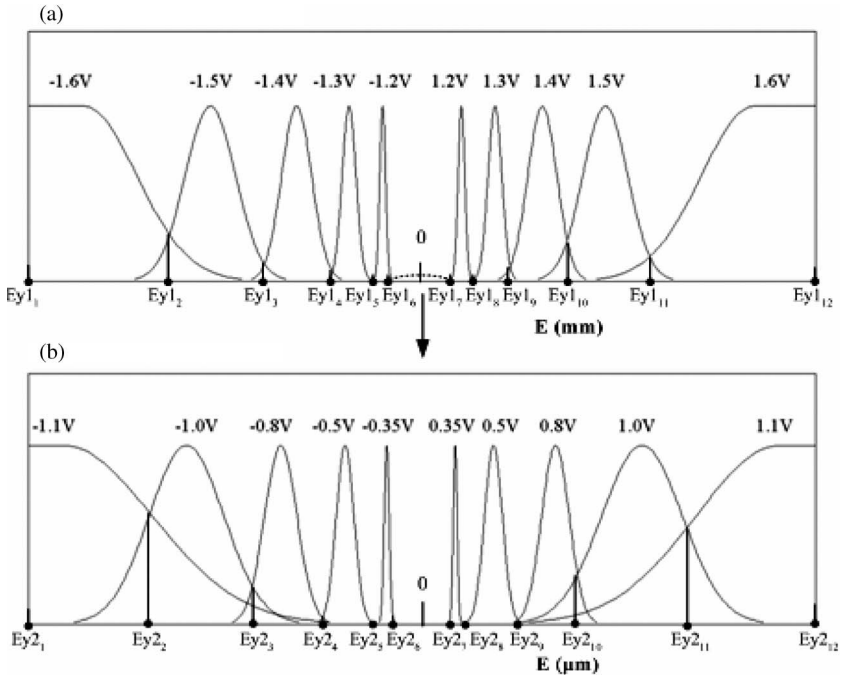

Fig. 11. Control areas of two stages on the Y-axis. (a) Area of coarse tuning. (b) Area of fine tuning.

into 0 V, and the LPAT stops and remains stationary for 20 ms. The errors between the current position and the target position are then calculated. These driving processes continue until the preceding error is ≤ 0.02 and ≥ -0.02 μm. Since the LPAT has remained in a static state, the effects of the dynamic change in error can be avoided. Hence, the LPAT can be precisely positioned at ± 0.02 μm easily.

The controller proposed in this paper can also automatically provide the "compensating voltage" added to the smallest driving voltage, including ± 1.3 V of the X-axis and ± 1.2 V of the Y-axis in CTS as well as ± 0.3 V of the X-axis and ± 0.35 V of the Y-axis in FTS. The preceding "starting voltage" varies with time for different temperatures and static frictions produced by the vertical load of the LPAT. Hence, a tremendous change in temperature or a large increase in vertical load applied on the LPAT will cause the starting voltages to exceed the corresponding smallest driving voltages. This will stop the movement of the LPAT although the driving voltage is still sent to the driver continuously. Consequently, the positioning control will never finish. To prevent such from happening, during the positioning process, if the LPAT remains stationary for 0.05 s in CTS or for 0.15 s in FTS, the controller will automatically provide the compensating voltage, beginning from 0 V and gradually increasing in positive direction or decreasing in negative direction at intervals of 0.02 V in CTS or at intervals of 0.01 V in FTS, to combine with the current driving voltage sent to the driver until the LPAT starts moving again.

VI. Experimental Results and Discussion

Since the LPAT is driven by a lead zirconium titanate (PZT) actuating fingertip instead of the PZT element directly, it has a larger moving travel. Moreover, the resolution of the linear scale used in the experiment is only 20 nm, and the LPAT can also be driven for a smaller distance. For all the experiments, from small to large travel, three targets, including ± 0.1 μm, ± 0.1 mm, and ± 20 mm, are selected as the end positions on the X- and Y-axes for RBM positioning control. During the positioning procedure, the rise time T_r, the maximum overshoot percent M_p, and the 2% settling time T_s of the transient response in time domain as well as the steady-state error $E_{\rm ss}$ are calculated and recorded to evaluate the control performance of the proposed RBM controller [15]. The main advantages of the proposed approach, compared with other methods, are the significant improvements of the system's performance, specifically on error minimization. The error is close to zero, and this small error is also achievable for all tested stroke distances. The simplicity and its robustness are the main advantages of this approach. The performance's comparison of the proposed method to other methods is shown in Table IV.

The error is still the same (ranging from -0.02 to 0.02 μm) for all tested stroke distances, including ± 0.1 μm, ± 0.1 mm, and ± 20 mm. This means that the proposed approach is much better than all the other methods, as listed in Table IV.

A. Experimental Results of Positioning Targets of 0.1 and -0.1 μm

Since the target of 0.1 μm is less than 20 μm, the controller skips CTS and directly enters FTS. As seen in Fig. 12(a) and (b), a fine voltage scheme of 0.3 V is selected 11 times by the X-axis RBM to drive the LPAT toward the target. Similarly, as shown in Fig. 12(c) and (d), a fine voltage scheme of 0.35 V is selected seven times by the Y-axis RBM to drive the LPAT toward the target.

Because the target of -0.1 μm is greater than -20 μm, the controller directly enters FTS without executing CTS. For the X-axis, as shown in Fig. 13(a) and (b), -0.1 μm is a short

TABLE IV
COMPARISON OF DIFFERENT POSITIONING CONTROL METHODS

Author(s)	Methods and Characteristics	Results obtained
Sung et al. [10]	Three-stage fuzzy logic motion control	Steady-state error: 0.1 to 0.2 μm
Sung et al. [10]	PID control, Kp = 1.9, Kd = 0.00013, Ki = 0.0008	Steady-state error: 0.5 to 2.5 μm
Wai et al. [11]	Using a double-inductance double-capacitance resonant driving circuit and a four-layer sliding-mode fuzzy- neural-network controller	The max. tracking error is 1.06mm
Wai et al. [12]	Using a supervisory genetic algorithm (SGA) composed of two parts	The maximum tracking error is 0.66mm.
Wai et al. [13]	Using an adaptive grey control to achieve a grey uncertainty predictor and estimate the lumped uncertainty on line.	A tracking error is about 1.5mm.
Lin et al. [14]	Using an adaptive cerebellar-model-articulation-controller-based supervisory control system	The maximum error is about 0.84mm.
Proposed method	Using multistage rule-based precision positioning control method	Steady state error: -0.02 to 0.02 μm

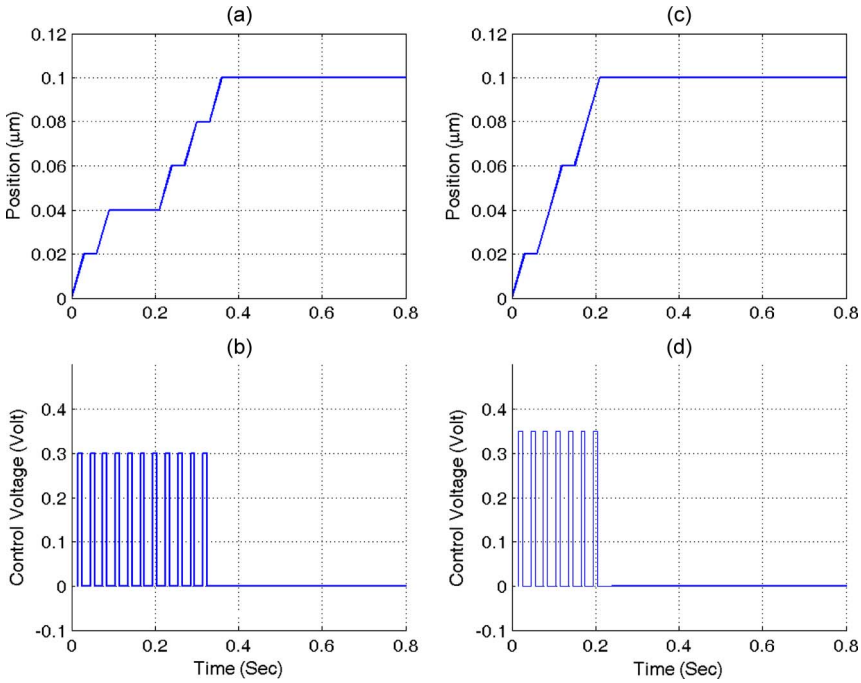

Fig. 12. Position responses to control voltages for two axes for target of 0.1 μm. (a) X-axis position versus time. (b) X-axis voltage versus time. (c) Y-axis position versus time. (d) Y-axis voltage versus time.

distance, and the smallest fine voltage schemes of -0.3 and $+0.3$ V are alternately selected to actuate the LPAT about six times to reach the target accurately. However, the positioning process of the Y-axis is a little different from that of the X-axis, as plotted in Fig. 13(c) and (d). The same fine voltage scheme of -0.35 V is selected 11 times by the Y-axis RBM to reach the target step by step. The measured results of the positioning targets of 0.1 and -0.1 μm for the X- and Y-axes are shown in Table V.

B. Experimental Results of Positioning Targets of 0.1 and −0.1 mm

A positioning target of 0.1 mm is shown in Fig. 14(a) and (b), where a coarse voltage scheme of 1.4 V is initially selected by the X-axis RBM in CTS. It is then reduced to 1.3 V to actuate the LPAT to exceed the target promptly, and the position error becomes negative. The coarse voltage scheme is then converted into the negative fine voltage scheme of -1.1 to -0.4 V to accurately reach the target. On

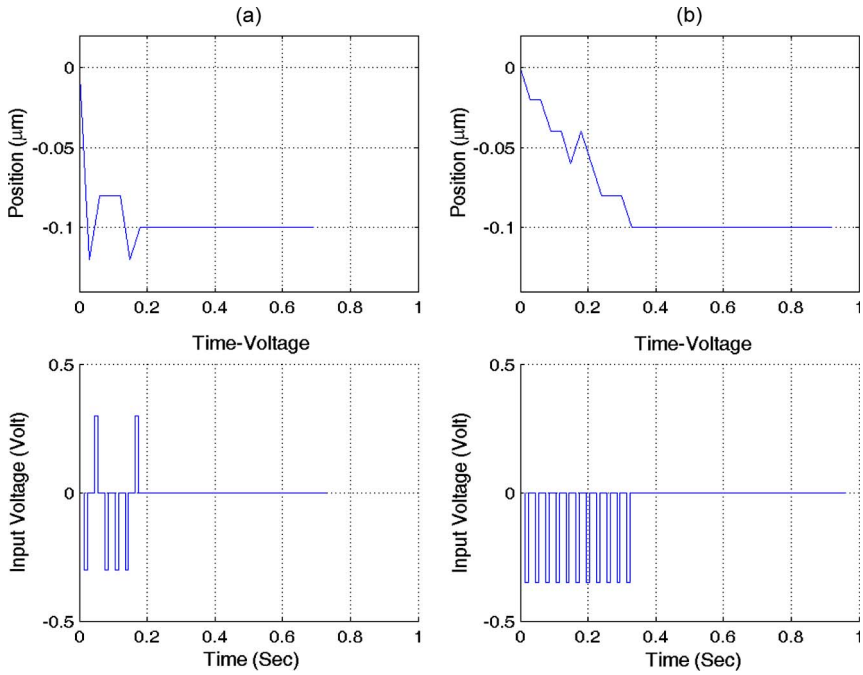

Fig. 13. Position responses to control voltages for two axes for target of -0.1 μm. (a) X-axis time position. (b) Y-axis time position.

TABLE V
EXPERIMENTAL RESULTS OF X- AND Y-AXES

	Target	0.1μm	-0.1μm	0.1mm	-0.1mm	20mm	-20mm
X-axis	T_r (sec)	0.33	0.15	0.03	0.04	1.25	1.24
	T_s (sec)	0.36	0.18	0.11	0.48	1.57	1.64
	M_p (%)	0	20	11.6	7.3	0.1	0
	E_{ss} (μm)	0	0	0	0.02	0	0
Y-axis	T_r (sec)	0.15	0.27	0.03	0.02	1.19	1.40
	T_s (sec)	0.21	0.33	0.08	0.24	1.38	1.84
	M_p (%)	0	0	6.4	5.1	0.2	0
	E_{ss} (μm)	0	0	0.02	0.02	0.02	0

the other hand, in Fig. 14(c) and (d), a coarse voltage scheme of 1.2 V is initially selected by the Y-axis rule base to actuate the LPAT promptly to approach the target, and then converted into a fine voltage scheme, oscillating six times to reach the target.

Since the target of -0.1 mm is smaller than -0.02 mm, as shown in Fig. 15(a) and (b), a coarse voltage scheme of -1.3 V is initially selected by the X-axis RBM to promptly drive the LPAT to approach the target. It is then converted into a fine voltage scheme to precisely reach the target. The positioning process of the Y-axis is similar to that of the X-axis, except that the initial coarse voltage scheme is -1.2 V instead, as shown in Fig. 15(c) and (d), and all the fine voltage schemes in FTS are positive. The measured results of the positioning targets of 0.1 and -0.1 mm for the X- and Y-axes are shown in Table V.

C. Experimental Results of Positioning Targets of 20 and −20 mm

Since the 20-mm target of the X-axis is of a long distance, as shown in Fig. 16(a) and (c), the maximum coarse voltage scheme of 1.7 V is selected by the X-axis RBM in CTS to drive the LPAT for about 1.4 s, then gradually reduced to 1.3 V, and finally converted into fine voltage scheme after the position error becomes smaller than 0.02 mm. The transient response dies down promptly and then converges gradually to reach the target finally. The position errors between -20 and 0.1 μm are shown in Fig. 16(b), which can describe the final detailed motion approaching the target. The 20-mm positioning control of the Y-axis is plotted in Fig. 16(d) and (f). It is similar to that of the X-axis. The maximum coarse voltage scheme of 1.6 V is also selected by the Y-axis rule base to drive the LPAT for about 1.2 s, then gradually reduced to 1.2 V, and finally converted into fine voltage scheme after the position error becomes smaller than 20 μm. The driving process before reaching the target is plotted in detail in Fig. 16(e), where the LPAT goes beyond the target, retreats, and finally reaches the target.

Since -20 mm is of a long distance, as shown in Fig. 17(a) and (c), the maximum coarse voltage scheme of -1.7 V is selected by the X-axis RBM in CTS to drive the LPAT continuously for about 1.3 s at maximum velocity. It is gradually increased to -1.3 V and then switched to fine voltage scheme to precisely reach the target. Similarly, the driving process before reaching the target is plotted in Fig. 17(b), which depicts the step-by-step approach of the LPAT. The positioning process of the Y-axis is shown in Fig. 17(d) and (f). In CTS, the maximum coarse voltage scheme of -1.6 V is selected by the Y-axis RBM to drive the LPAT continuously for about 1.7 s at maximum velocity. It is gradually increased to -1.2 V and then converted into fine voltage scheme to reach the target accurately. The driving process before the Y-axis reaches the target is plotted in detail in Fig. 17(e). As can be seen, the LPAT steadily moves toward the target without oscillation. The measured results of the positioning

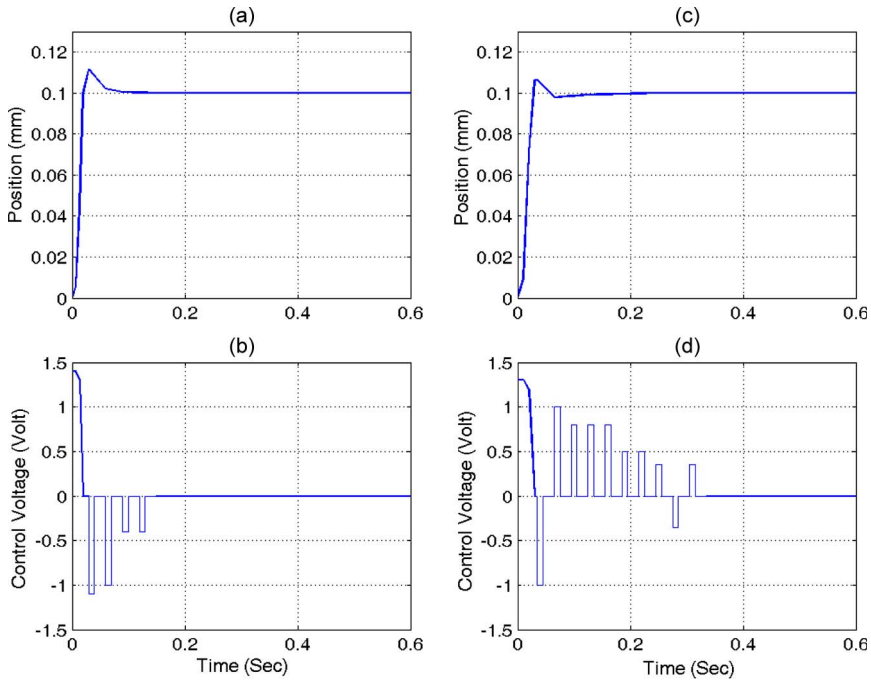

Fig. 14. Position responses to control voltages for two axes for target of 0.1 mm. (a) X-axis position versus time. (b) X-axis voltage versus time. (c) Y-axis position versus time. (d) Y-axis voltage versus time.

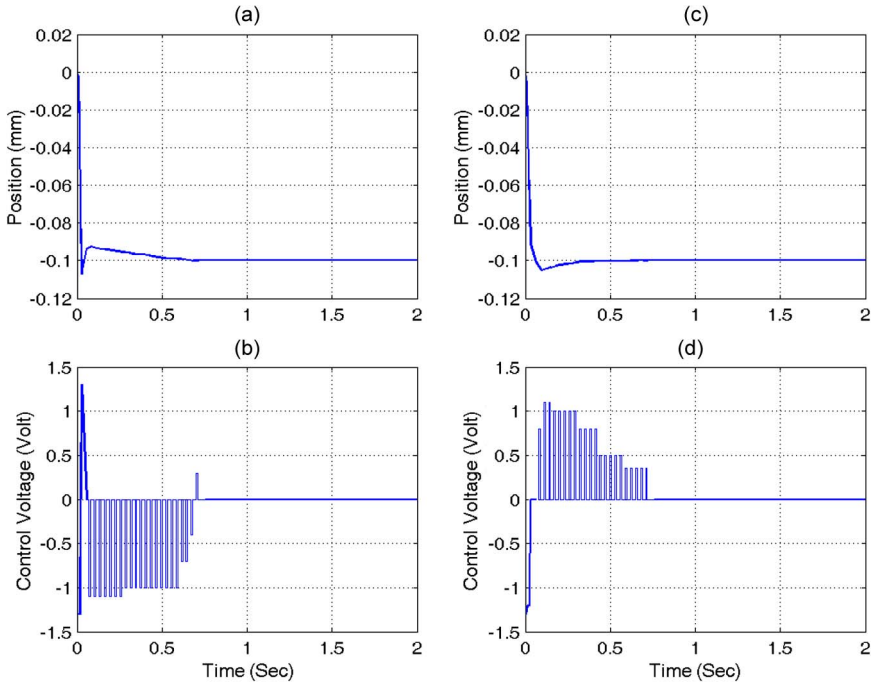

Fig. 15. Position responses to control voltages for two axes for target of -0.1 mm. (a) X-axis position versus time. (b) X-axis voltage versus time. (c) Y-axis position versus time. (d) Y-axis voltage versus time.

targets of 20 and -20 mm for the X- and Y-axes are shown in Table V.

VII. Conclusion

A piezoelectric actuator usually has the disadvantages of suffering from serious hysteresis behavior and nonlinearity properties, which are difficult to overcome using conventional control strategies. This paper uses an intelligent approach based on experience and statistical methods to establish the rule base of positioning control instead of a complex mathematical model. For instance, it was found that gain tuning can be omitted and still achieve highly-accurate results, outperforming the work by others [10]–[14]. The experimental results of 12 positioning targets of the two axes are displayed in Table V, showing the rise time T_r, maximum overshoot percent M_p, and 2% settling time T_s of the transient response as well as steady-state error $E_{\rm ss}$. As can be seen, the time of 10 T_r and 10 T_s

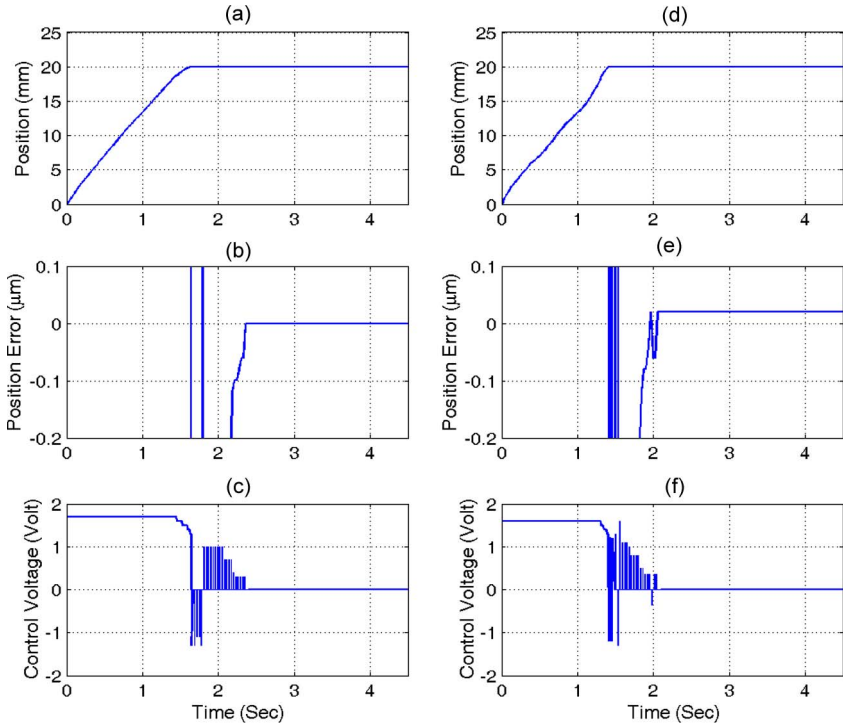

Fig. 16. Position responses to control voltages for two axes for target of 20 mm. (a) X-axis position versus time. (b) X-axis position error. (c) X-axis voltage versus time. (d) Y-axis position versus time. (e) Y-axis position error. (f) Y-axis voltage versus time.

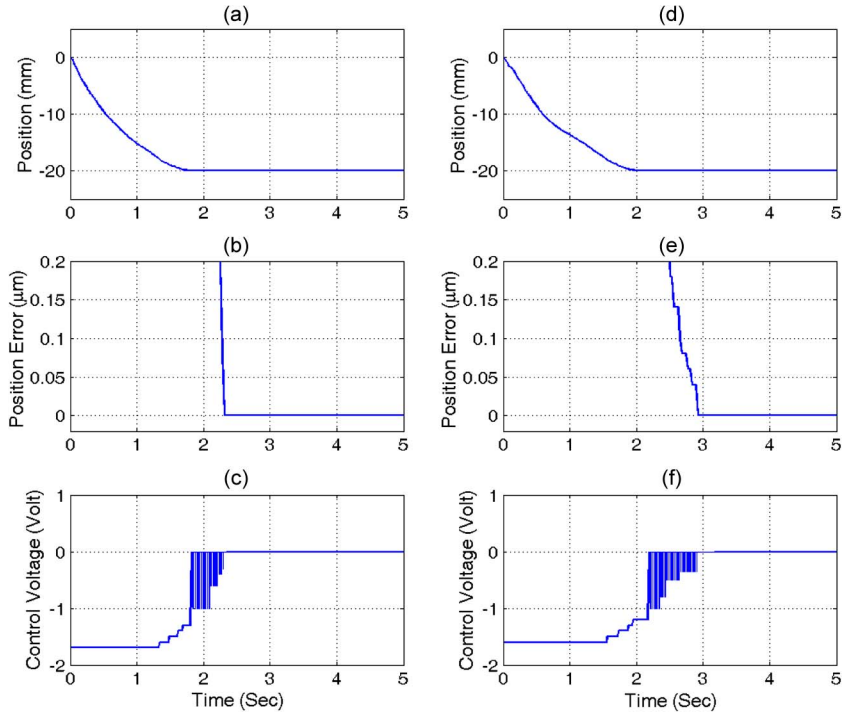

Fig. 17. Position responses to control voltages for two axes for target of -20 mm. (a) X-axis position versus time. (b) X-axis position error. (c) X-axis voltage versus time. (d) Y-axis position versus time. (e) Y-axis position error. (f) Y-axis voltage versus time.

are less than 0.6 s except for the two longer travel positioning control targets of 20 and -20 mm. Although more time is needed for the latter targets, the positioning control can still reach steady state within 2 s. As for M_p, as seen in Table V, the measurement results of 10 of 12 M_p are less than 10% of setpoints, and all other measurement results are within 20% of setpoints. The experimental results indicate that the proposed RBM controller can achieve fast transient response and good stability from easy decay to convergence by means of proper overshoot.

As seen in Table V, the steady-state error of each selected positioning target can easily reach ± 0.02 μm for the reason

described in Section V. The errors between the current position and the target position are calculated in FTS, when the LPAT has been in a stationary state, and thus, the influence of dynamic error changes on the controller can completely be avoided. Hence, the proposed LPAT can easily achieve accurate positioning of ± 0.02 μm.

In general, the absolute error is found to be 0.02 μm for both $\pm$ 0.1 and ± 20 μm ranges. However, the relative errors are 10% and 0.05%, respectively. This means that the error is too high for the ± 0.1 μm motion range, whereas it is very good for a ± 20 μm motion range. Considering the measurement needs for much smaller motion ranges in today's technology, the method will not be suitable for nanomeasurements, whereas it may be preferable for micrometer (microelectromechanical systems) measurement ranges.

REFERENCES

[1] S. C. Kim and S. H. Kim, "A precision linear actuator using piezoelectrically driven friction," *Mechatronics*, vol. 11, no. 8, pp. 969–985, Dec. 2001.

[2] S. H. Chang, C. K. Tseng, and H. C. Chien, "Ultra-precision XYθZ piezo-micropositioner Part I: Design and analysis," *IEEE Trans. Ultrason., Ferroelectr., Freq. Control*, vol. 46, no. 4, pp. 897–905, Jul. 1999.

[3] S. H. Chang, C. K. Tseng, and H. C. Chien, "Ultra-precision XYθZ piezo-micropositioner Part II: Experiment and performance," *IEEE Trans. Ultrason., Ferroelectr., Freq. Control*, vol. 46, no. 4, pp. 906–912, Jul. 1999.

[4] W. Lin, N. K. Ann, and L. E. Ng, "Concepts for a class of novel piezoelectric self-locking long-stroke actuators," *Precis. Eng.*, vol. 26, no. 2, pp. 141–154, Apr. 2002.

[5] Y. T. Liu, R. F. Fung, and C. C. Wang, "Precision position control using combined piezo-VCM actuators," *Precis. Eng.*, vol. 29, no. 4, pp. 411–422, Oct. 2005.

[6] M. Negnevitsky, *Artificial Intelligence*, 2nd ed. Reading, MA: Addison-Wesley, 2005, p. 30.

[7] S. J. Kang, C. H. Woo, H. S. Hwang, and K. B. Woo, "Evolutionary design of fuzzy rule base for nonlinear system modeling and control," *IEEE Trans. Fuzzy Syst.*, vol. 8, no. 1, pp. 37–45, Feb. 2000.

[8] H. L. Zhao and M. Qing, "Method to obtain effective rule base for unknown nonlinear system," in *Proc. Process. 2nd Int. Conf. Mach. Learn. Cybern.*, 2003, vol. 2–5, pp. 519–524.

[9] V. G. Moudgal, K. M. Passino, and S. Yurkovich, "Rule-based control for a flexible-link robot," *IEEE Trans. Control Syst. Technol.*, vol. 2, no. 4, pp. 392–405, Dec. 1994.

[10] M. Y. Sung and S. J. Huang, "Fuzzy logic motion control of a piezoelectrically actuated table," *Proc. Inst. Mech. Eng., Part I: J. Syst. Control Eng.*, vol. 218, no. 5, pp. 381–397, 2004.

[11] R. J. Wai and J. D. Lee, "Intelligent motion control for linear piezoelectric ceramic motor drive," *IEEE Trans. Syst., Man, Cybern. B, Cybern.*, vol. 34, no. 5, pp. 2100–2111, Oct. 2004.

[12] R. J. Wai and K. H. Su, "Supervisory control for linear piezoelectric ceramic motor drive using genetic algorithm," *IEEE Trans. Ind. Electron.*, vol. 53, no. 2, pp. 657–673, Apr. 2006.

[13] R. J. Wai, "Adaptive Grey control for hybrid resonant driving linear piezoelectric ceramic motor," *IEEE Trans. Ind. Electron.*, vol. 53, no. 2, pp. 640–652, Apr. 2006.

[14] C. M. Lin and Y. F. Peng, "Adaptive CMAC-based supervisory control for uncertain nonlinear systems," *IEEE Trans. Syst., Man, Cybern., Part B: Cybern.*, vol. 34, no. 2, pp. 1248–1260, Apr. 2004.

[15] C. M. Douglas and C. R. George, *Applied Statistics and Probability for Engineers*. New York: Wiley, 2002.

[16] G. B. Thomas, D. M. Roy, and H. L. John, *Mechanical Measurements*., 5th ed. Reading, MA: Addison-Wesley, 1995.

[17] W. Bolton, *Control Engineering*, 2nd ed. White Plains, NY: Longman, 1999.

[18] J. S. Taur, G. H. Lee, and C. W. Tao, "A multi-stage design of adaptive fuzzy controllers for time-delay systems with unknown models," *Int. J. Syst. Sci.*, vol. 38, no. 5, pp. 433–449, May 2007.

[19] J. Y. Keller, M. Darouach, and L. Caramelle, "Kalman filter with unknown inputs and robust multi-stage filter," *Int. J. Syst. Sci.*, vol. 29, no. 1, pp. 41–47, Jan. 1998.

[20] Z. Hasiewicz, "Multi-stage procedure for parameter estimation in large-scale interconnected linear zero-memory systems," *Int. J. Syst. Sci.*, vol. 19, no. 3, pp. 497–516, 1988.

Hendro Nurhadi received the Dipl.-Ing.(FH) degree from the University of Applied Science Georg-Simon-Ohm Fachhochshule Nuremberg, Nuremberg, Germany, in 2001 and the Ph.D. degree from the National Taiwan University of Science and Technology (NTUST), Taipei, Taiwan, in 2009.

He is currently with the Department of Mechanical Engineering at Institute of Technology Sepuluh Nopember (ITS), Surabaya, Indonesia, and a Director of Research Group for Intelligent Motion Systems and Identification (IMSI), Mechanical Engineering at Institute of Technology Sepuluh Nopember (ITS), Surabaya, Indonesia. He has authored numerous international journal papers and international conferences. His research interests and consulting activities are in the areas of motion control and automation, advanced mechatronics, automated optical inspection (AOI), machine tool dynamics, automation of manufacturing processes, computer-aided design and manufacturing, optimization applications, digital signal processing, and artificial intelligence.